EMSP Project Final Report

Project Title:

Investigation of Microscopic Radiation Damage in Waste Forms Using ODNMR and AEM Techniques

Project ID: 55367

Principal Investigator:

Guokui Liu
Chemistry Division
Argonne National Laboratory
9700 South Cass Avenue
Argonne, Illinois 60439
Telephone: 630-252-4630
E-mail: gkliu@anl.gov

Co-Investigators:

Jianshu Luo
Chemical Technology Division
Argonne National Laboratory
9700 South Cass Avenue
Argonne, Illinois 60439
Telephone: 630-252-7898
E-mail: luo@cmt.anl.gov

James Beitz
Chemistry Division
Argonne National Laboratory
9700 South Cass Avenue
Argonne, Illinois 60439
Telephone: 630-252-7393
E-mail: beitz@anl.gov

Other Contributors at ANL:

Shutao Li
Clayton Williams
Victor Zhorin

INVESTIGATION OF MICROSCOPIC RADIATION DAMAGE IN WASTE FORMS USING ODNMR AND AEM TECHNIQUES

I. Research Objective 2
II. Summary of Project Accomplishment 2
III. Radiation Effects in ^{244}Cm-Loaded Orthophosphates 3
a. Defect clusters 4
b. Metastable lattice distortion 6
c. Molecular dynamics simulation of damage and recovery 7
d. Defect aggregation and bubble formation 8
d. Defect aggregation and bubble formation 9
IV. Actinides in Borosilicate Glass 11
a. Local structure of actinides in borosilicate glass 11
b. Radiation damage in borosilicate glass 13
V. Implications 14
VI. Publications 15
VII. Reference 16

I. Research Objective

This project seeks to understand the microscopic effects of radiation damage in nuclear waste forms. Our approach to this challenge encompasses studies of ceramics and glasses containing short-lived alpha- and beta-emitting actinides with electron microscopy, laser and X-ray spectroscopic techniques, and computational modeling and simulations. In order to obtain information on long-term radiation effects on waste forms, much of our effort is to investigate α-decay induced microscopic damage in 18-year old samples of crystalline yttrium and lutetium orthophosphates that initially contained ~1(wt)% of the alpha-emitting isotope ^{244}Cm (18.1 y half life). Studies also are conducted on borosilicate glasses that contain ^{244}Cm, ^{241}Am, or ^{249}Bk, respectively. We attempt to gain clear insights into the properties of radiation-induced structure defects and the consequences of collective defect-environment interactions, which are critical factors in assessing the long-term performance of high-level nuclear waste forms [Ewing et al. 1995, Weber et al. 1998].

II. Summary of Project Accomplishment

We have reached our project goals with experimental results and observations that characterize the microscopic and long-term effects of radiation damage in nuclear waste forms. Laser and X-ray spectroscopic techniques and analytic electron microscopy were used as our primary experimental tools for probing local structure and structural changes. In this project, computational modeling and simulation of experimental results were essential for providing fundamental understanding of the properties of actinides in disordered solids and interpreting complicated effects of radiation damage and recovery.

We extensively studied radiation-induced structural damage in crystalline orthophosphates that were doped with ^{244}Cm. The samples were synthesized 18 year ago and stored since then at room temperature. Before our experiments were conducted, almost half of the originally doped 1 wt% ^{244}Cm already had decayed to ^{240}Pu and the total radiation dose reached ~ $5X10^{19}$ decay-events/g in the samples. The phenomenon of radiation-induced cascade displacements in crystalline and glassy materials is generally understood. As demonstrated by heavy-ion-implantation experiments, when the dose of the radiation source increases, crystalline orthophosphates become amorphous at room temperature. However, amorphization was not observed in the samples that we studied, although the total dose was sufficiently high that such amorphization would have been expected. In the orthophosphates that we studied, atomic displacements induced by α-decay events did not persist with the exception that residual lattice distortion and stress were left as a result of damage and recovery. We have shown that the average residual lattice distortion is smaller than the atom size and can be annealed at higher temperatures. Our observation is consistent with the discovery in geophysics that crystalline structure is largely preserved in natural zircon and phosphates after significant accumulated radiation dose from thorium and uranium decays over millions of years on the surface of the earth.

Instead of a crystalline to amorphous transition, we observed numerous bubbles and isolated defect clusters of nanometer size in the aged phosphate samples [Liu et al. 1998a,

Luo and Liu 2000]. We attribute the nanoclusters to fission tracks and bubbles to the aggregation of α-generated helium atoms. The bubbles and defect clusters were found to coalesce under electron beam irradiation. Our work show that the important parameters for the long-term performance of high-level nuclear waste forms are not only the total number of point defects (vacancies and interstitials) generated by cascade displacement but also the distribution of their population in clusters and the form and mobility of these clusters. Formation and mobilization of microscopic bubbles and cracks are important potential degradation mechanisms that may cause radionuclide release from the disposed waste forms.

Samples of borosilicate glass that contain natural uranium or short-lived actinide isotopes of ^{241}Am, ^{244}Cm, and ^{249}Bk were prepared as model waste forms and studied in this project with selective laser excitation and X-ray spectroscopy [Liu et al. 2000a]. Our studies have shown that, in borosilicate glasses, actinide ions have ordered structure as to their nearest neighbors. This property allows us to monitor radiation-induced structural damage. After preparation of the glass samples, selective laser excitation was conducted to probe the local environments of the actinide ions. The same measurements were repeated later to monitor the evolution of radiation-induced damage. Extended X-ray absorption fine structure (EXAFS) spectra of the actinide ions in the glass samples also were recorded and analyzed in this project. Based on these spectroscopic results, we have established a framework for analyzing local structure in this model waste form.

Radiation damage of solid phase materials is an extremely complicated process. Our work focused on microscopic structural damage that was induced by α-decay. In order to accurately assess and optimize the long-term performance of high-level nuclear wastes after disposal, a predictive understanding of defect aggregation and chemical segregation in waste forms must be achieved. To achieve such predictive understanding, more detailed studies are required. We believe that contemporary technologies such as element-resolved electron microscopic analysis and computational modeling and simulations should provide significant opportunities to tackle these problems more satisfactorily.

III. Radiation Effects in ^{244}Cm-Loaded Orthophosphates

Orthophosphates containing ^{244}Cm were chosen for detailed study in this project because: (i) radiation damage was accelerated by the short-lived α-decay isotope ^{244}Cm, and considerable radiation dose already had accumulated in the samples available to us, and (ii) similar to zircon, lanthanide phosphates are candidate ceramic nuclear waste forms due to their resistance to radiation [Boatner et al. 1981]. The ^{244}Cm-loaded $LuPO_4$ and YPO_4 single crystals that we studied were grown in 1980 at Oak Ridge National Laboratory using a flux method [Abraham and Boatner 1982]. These single crystals initially had a ^{244}Cm concentration of ~1 wt%. After 18 years of α-decay, half of the initially doped ^{244}Cm ions became ^{240}Pu, and simultaneously, various dynamical interactions facilitated defect development as well as lattice recovery. Therefore, the phenomena that we observed in the phosphate samples should closely reflect long-term radiation effects in ceramic waste forms. To investigate atomic level radiation damage and aging effects on defect development,

electron diffraction (ED) and transmission electron microscopy (TEM) were conducted. Laser spectroscopic experiments were conducted before and after heat treatment (annealing at 500 ^{o}C for 12 hours) of the samples [Liu et al. 1998c, 2000b].

Samples for TEM examination were prepared with ultramicrotomy [Luo and Abraham 1999]. Sections that were 50 nm thick were cut with a Reichert-Jung ultramicrotome. Because of the anisotropic structure of $LuPO_4$ and YPO_4 crystals, attempts were made to section the crystal along different orientations. The transverse sections were the most successful, whereas longitudinal sections were difficult to make. Transmission electron microscopy was performed with a JEOL 2000FX unit operating at 200 kV and equipped with an energy dispersive x-ray spectrometer (EDS). Selected area electron diffraction (SAED) was employed along with bright- and dark-field imaging. The chemical analyses by EDS were performed with a 15-nm focused electron beam, which corresponds roughly with the spatial resolution of the analysis. The crystallinity of the area examined was determined with SAED as well as with direct lattice imaging.

a. Defect clusters

Except for the presence of individual defect clusters, amorphization was not observed in the phosphate samples that we studied. Figure 1 shows SAED patterns obtained from a fairly large area (about 0.1 x 0.1 µm) in the ^{244}Cm-doped $LuPO_4$ and YPO_4 samples. Sharp diffraction spots were dominant in the pattern, indicating that the material remained largely crystalline. Some faint sharp rings were also present in the SAED pattern. However, there was little radial diffusion crossing the diffraction spots. This finding indicates no prominent amorphous component in the crystal. The presence of the ring structure in the diffraction

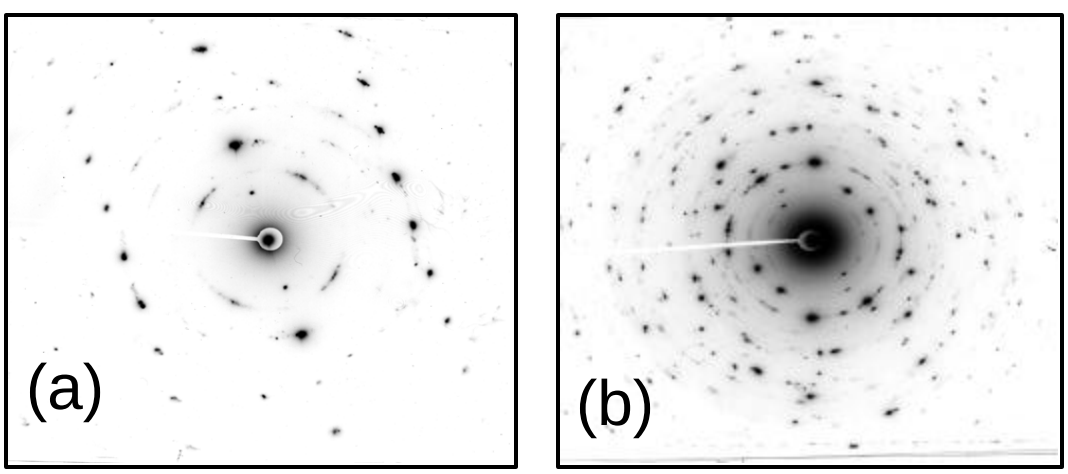

Fig. 1 SAED images of (a) ^{244}Cm:$LuPO_4$ and (b) ^{244}Cm:YPO_4.

pattern is attributed to the disruption of the sample during microtomy, which is a well known artifact that can occur during sectioning brittle materials [Reid and Beesley 1991]. Similar rings were also observed in the nondoped $LuPO_4$ samples that had been sectioned under the same conditions.

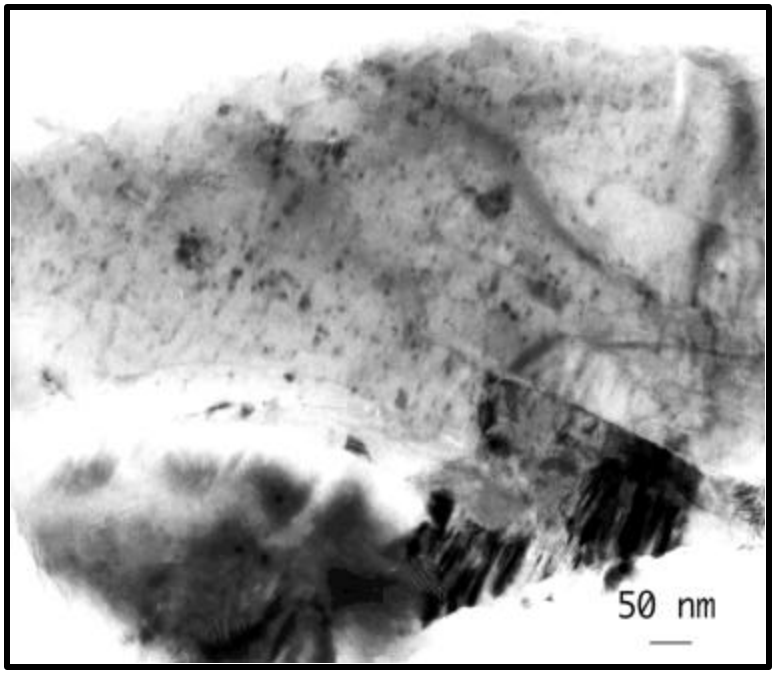

Fig. 2 A TEM image of $^{244}Cm:YPO_4$.

Figure 2 shows bright-field TEM micrographs of the ^{244}Cm-doped YPO_4. Individual defect clusters were observable by their strain contrast. The clusters typically have diameters of 5-10 nm and may be related to highly disordered fission tracks that are produced by the ^{240}Pu recoil nucleus emitted during the alpha decay of ^{244}Cm. If these are fission tracks, the structural nature of these defects is not known but may be assumed to be amorphous, because fission fragments are known to induce amorphization in crystalline materials [Weber et al. 1998]. Analysis of the clusters with EDS and the focused electron beam showed no difference in composition from the surrounding areas. Weber et al.[1986] observed individual fission tracks with lengths of 2.5-5.0 nm in ^{244}Cm-doped $Gd_2Ti_2O_7$ and $CaZrTi_2O_7$ when the irradiation dose was relatively low ($< 10^{15}$ α-decay events mg^{-1}). At higher doses, the fission tracks were reported to overlap each other, and the samples became completely amorphous.

b. Metastable lattice distortion

In addition to isolated defect clusters that are observable in the TEM images, we found that smaller scale defects and lattice distortion exist in the samples that we studied. Although TEM revealed no lattice amorphization, the crystallinity in the 18-year old ^{244}Cm-doped phosphate samples is not nearly as good as the same compounds that were doped with non-radioactive lanthanide ions or much less radioactive actinides such as ^{248}Cm [Kot et al. 1993]. Based on our laser spectroscopic experiments and computational analyses, we attributed smaller scale defects and lattice distortion to the residuals of α-decay induced cascade displacements that were largely annealed at room temperature due to collective lattice dynamical interactions.

The line width of optical transitions between 5f states of the Cm ions is very sensitive to local structure. Structural disorder induces inhomogeneous line broadening. In a crystalline lattice, the line width for transitions between the crystal field levels of 5f electronic states is less than 100 GHz (3 cm^{-1}) at 4 K. The line width increases to 10^4 GHz and exhibits no clear crystal-field splitting in amorphous environments. We measured and analyzed the inhomogeneous line width of Cm^{3+} electronic transitions to determine the degree of lattice

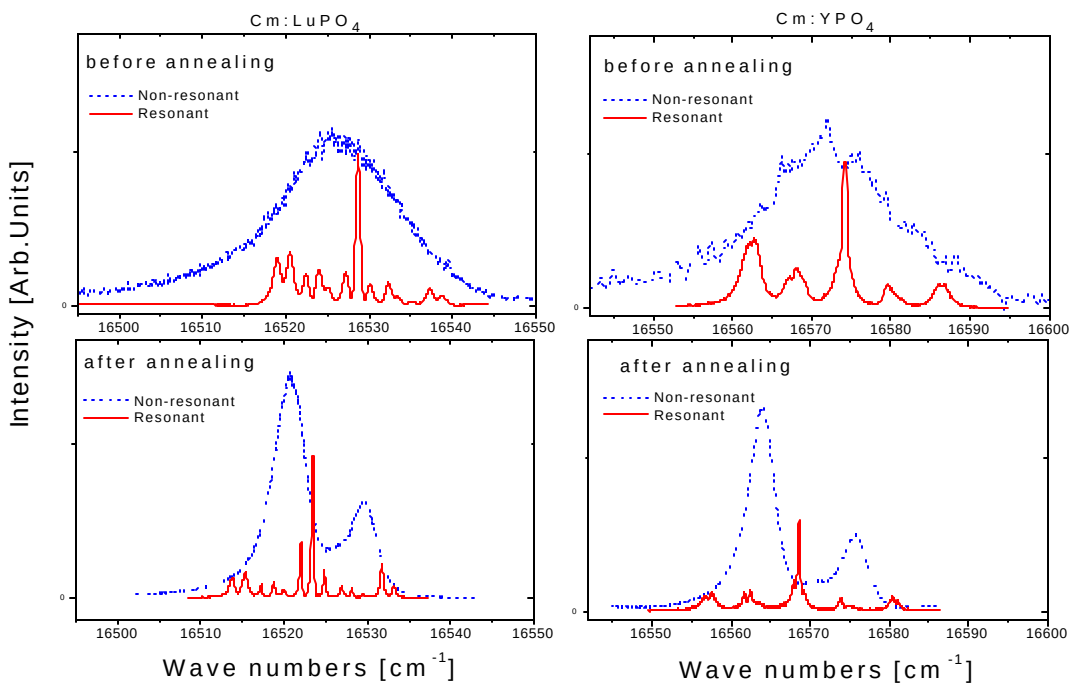

Fig. 3 Laser-induced fluorescence spectra for the $^6D_{7/2} \rightarrow {}^8S_{7/2}$ transition of Cm^{3+} in Cm^{3+}:$LuPO_4$ (left panel) and Cm^{3+}:YPO_4 (right panel). For comparison, the narrow-peak spectra (solid lines) that were obtained by site-selected resonant excitation do not exhibit inhomogeneous line broadening. The sharp peaks are due to the Cm^{3+} ground state splitting [Liu et al. 1998b,c]. The dashed curves that were obtained with nonresonant excitation show inhomogeneous broadening.

disorder in the α-decay-damaged phosphate crystals [Liu et al. 2000b]. Examples of these laser excitation and fluorescence spectra are shown in Fig. 3. The results indicate that the samples are still crystalline but there is evidence of lattice disorder due to radiation damage. The measured inhomogeneous line width was 20 cm^{-1} for both Cm-$LuPO_4$ and Cm-YPO_4 samples and reduced to less than 5 cm^{-1} after 12 h annealing at 500 ^oC. Our crystal-field calculation and Monte Carlo simulation determined that the observed 20 cm^{-1} line broadening corresponds to an average atom displacement less than 1/20 of the Cm atomic radius. Such small average displacements are not observable in TEM images.

c. Molecular dynamics simulation of damage and recovery

In order to understand the crystalline lattice damage and recovery mechanisms, cascade displacements and subsequent lattice recovery in Cm-doped $LuPO_4$ have been simulated using a molecular dynamics (MD) method. In our MD simulation, we included both two-body and three-body potentials, which is necessary for $LuPO_4$ and similar compounds because collective interatomic interactions are essential in the determination of chemical bonding and lattice dynamics properties. Our preliminary MD simulations on zircon and phosphate were carried out in a 500-MHz workstation computer that limited the simulated system to 10^4 atoms and knock-on energy of 20 keV.

Figure 4 shows the cascade evolution after a knock-on collision at a Lu atom in $LuPO_4$ along [111] direction. The cascade displacement reached its maximum domain size within 400 fs, and, then, lattice recovery after cascade displacements occurred along the boundary of the damaged domain. From 0.45 ps to 4 ps after the simulated α-decay event, the damaged domain shrank approximately 20%. It is evident that 4-ps after a collision event the system is far from reaching equilibrium. Atoms move intensively in the center of the domain and further lattice recovery continues. Our simulation also showed that, after cascade displacement and domain amorphization, lattice recovery is not complete and uniform. Point defects (interstitials and vacancies) appear in the recovered area of the damaged domain. In the case of $LuPO_4$, the heaviest Lu ions show much slower recovery action than the lighter P and O ions. Although PO_4 and LuO_8 polyhedra are likely reformed in the damaged domain, small distortion of these basic structures is evident. Therefore, in comparison with experimental observations, we found that the situation created in a MD simulation is generally the same as that revealed from TEM and laser spectroscopic experiments on the real damaged samples of $^{244}Cm:LuPO_4$. The lattice largely remained as crystalline but distortion and stress were left as residuals of α-decay-induced cascade displacements. The lattice damage and recovery dynamics are elucidated also in Fig.5, which shows the partial distribution functions of $LuPO_4$. One sees a clear lattice crystallinity recovery from 0. 5 ps to 18.8 ps after the cascade that occurred at t = 0. This preliminary MD simulation certainly shows promise for future work with more atoms and higher knock-on energy (up to the real α-decay recoiling energy of ~80 keV) that better reflects the actual HLW situations.

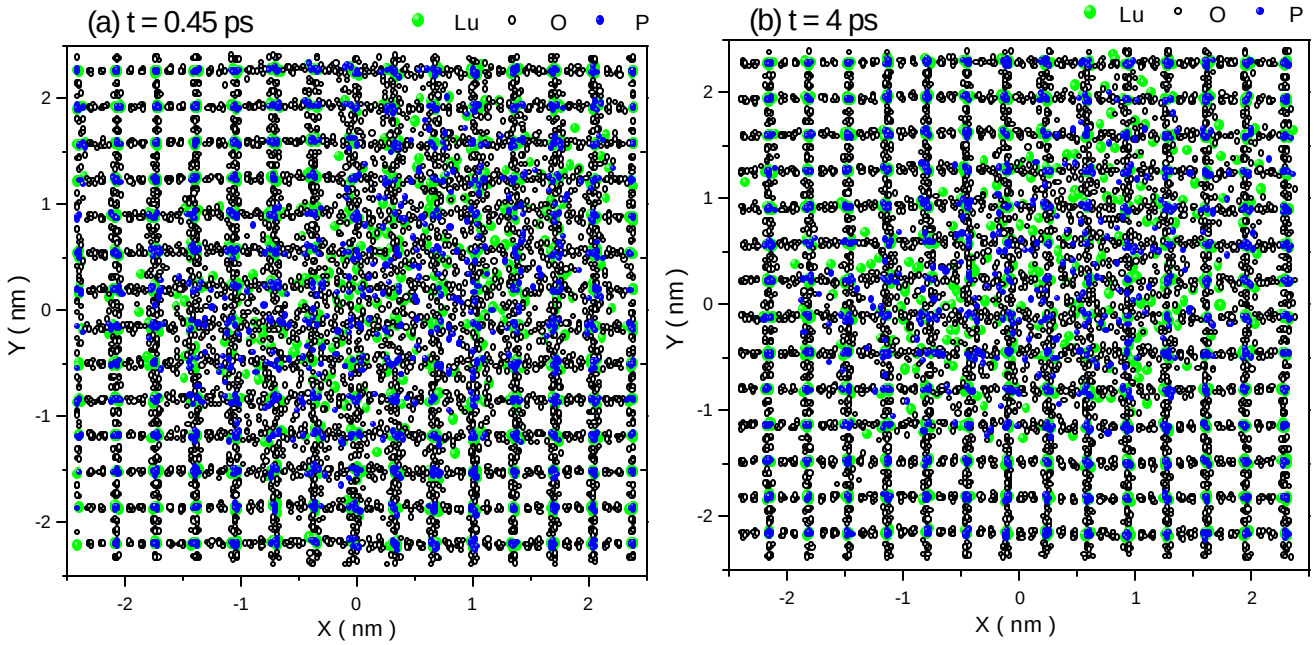

Fig. 4 MD simulation of $LuPO_4$ lattice (viewing along the c-axis) and α-decay-induced damage and lattice recovery. The first collision with knock-on energy of 20 keV was launched at t = 0 on a Lu atom along [111] direction. Before the cascade was initiated, the system reached equilibrium at 300 K. The total number of atoms in the simulated system was 8232, and the atoms on the surface were kept at 300 K.

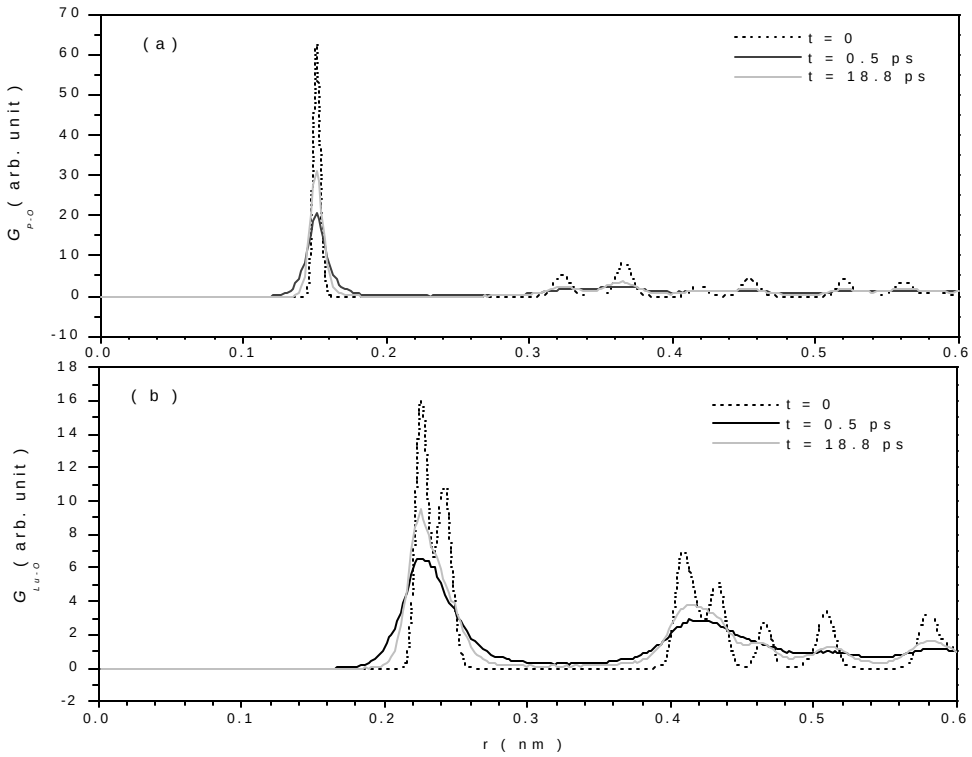

Fig. 5 MD simulation of partial radial distribution function, (a) for P-O pairs and (b) for Lu-O pairs, in crystalline $LuPO_4$ before and after cascade collisions as described in the text. The dashed curves are for the lattice before cascade (t=0). All atoms shown in Fig. 4 were accounted to obtain the data in this figure.

d. Defect aggregation and bubble formation

The results that are of most importance for predicting the long-term performance of high-level nuclear wastes are defect aggregation and bubble formation and mobilization. As shown in Fig. 5, the radiation effect observed in the ^{244}Cm-doped orthophosphates was the formation of bubbles [Luo and Liu 2000]. Most bubbles are roughly spherical, with sizes varying from 5 nm to 20 nm. In some cases, the bubbles appear to have coalesced and grown into larger ones. Analysis of the bubbles with EDS revealed no compositional changes from the surrounding crystalline areas. An enlarged section of Fig. 6 shows a lattice image of an isolated bubble and its vicinity. The (220) planes of $LuPO_4$ with d-spacing equal to 0.49 nm were resolved and imaged. The presence of regular stacking of the lattice planes is consistent with the electron diffraction data that showed that the materials remained largely crystalline. The lattice fringes were disrupted by the presence of the bubble, which forms an elongated ellipse of 25 nm x 70 nm. The boundary between the bubble and the orthophosphate crystal was rather sharp without formation of distorted or amorphous zones.

The formation of bubbles in self-radiated samples has been previously reported to occur in highly damaged natural minerals [Ewing and Headley 1983, Gong et al. 1997], as well as in nuclear waste glasses that contain actinides [Inagaki et al. 1992, Malow and Anderson 1979]. In most cases, formation of bubbles was associated with high actinide loading and/or long time periods [Weber 1990]. This is consistent with the high dose accumulated in the ^{244}Cm-doped sample. The exact nature and the chemical content of the bubbles are difficult

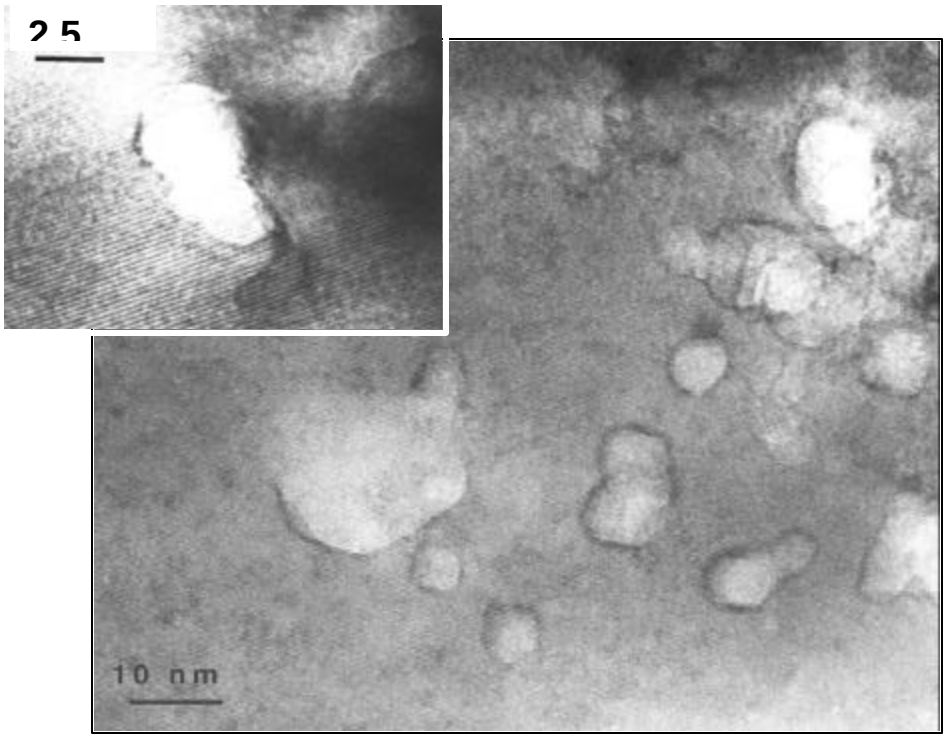

Fig. 6 TEM images of ^{244}Cm:$LuPO_4$ showing the presence of bubbles embedded in crystalline lattice. The insert image shows an isolated bubble and its crystalline vicinity.

to determine directly with TEM; nevertheless, the bubbles are assumed to contain mainly helium. This is because helium, resulting from the capture of two electrons by á-particles, must be accommodated interstitially or substitutionally in the crystal matrix. Because helium has very limited solubility in most ceramics [Weber et al. 1998], it may have diffused and coalesced to form helium bubbles. Although oxygen bubbles might also form as the result of oxygen bond disruption in the crystal due to radiation damage, it is unlikely they would accumulate in our sample. This is because any oxygen produced would quickly react with ^{240}Pu, the daughter product of the ^{244}Cm decay, which is a strong reducing agent.

Figure 7 shows a series of TEM images taken from the same area on the ^{244}Cm-doped YPO_4 sample at different intervals of exposure to the focused electron beam (about 200 nm in diameter). The area initially exhibited little contrast for the bubble presence. After the area was exposed to the electron beam for 100 s, areas of dark contrast appeared, likely corresponding to the diffusion and accumulation of the helium under the electron beam. After longer exposure (350 s), the bubbles appeared to regroup, grow larger, and become stable spherical shapes. After 1,000 s, the bubbles showed well-defined contours, suggesting that they may have broken after growing larger than the sample thickness (about 50 nm). During the whole experiment, the area under analysis remained crystalline, as determined with electron diffraction. Similar phenomenon was observed also in ^{244}Cm-doped $LuPO_4$.

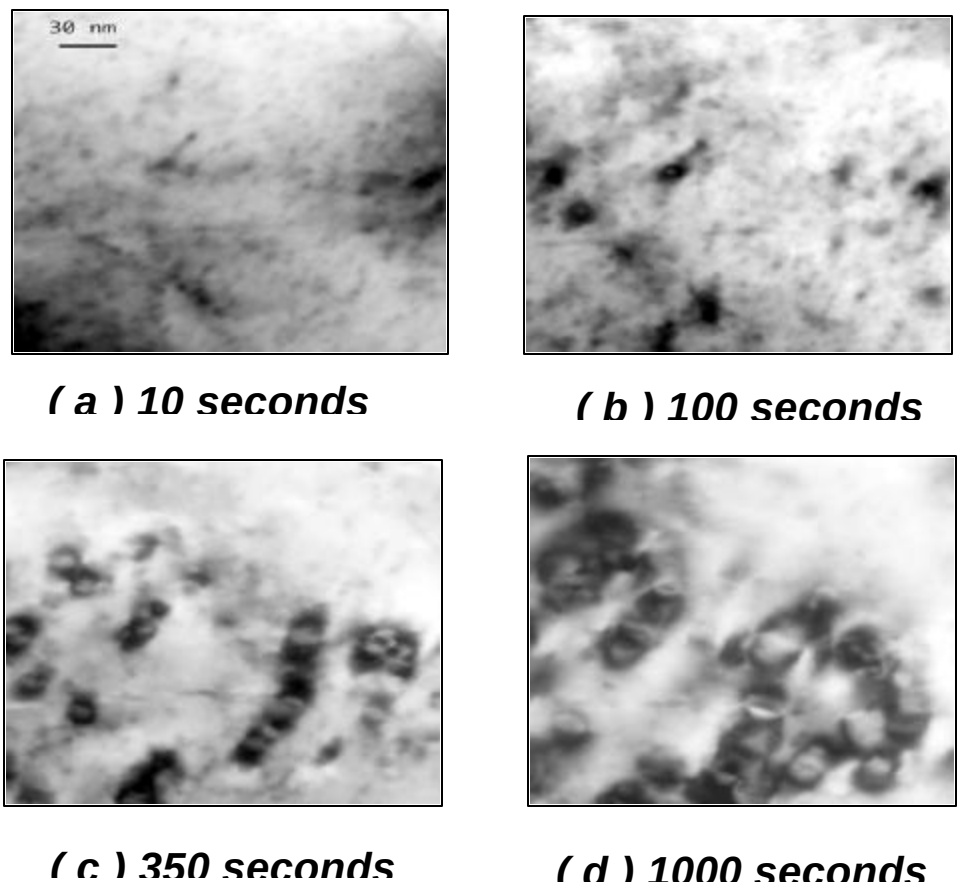

Fig. 7 When exposed to an electron beam in a TEM scope, bubbles form and aggregate in a 18-y old sample of (1 wt%) ^{244}Cm:YPO_4. The current density was approximately $1.5X10^{-16}$ A/cm^2.

IV. Actinides in Borosilicate Glass

Our work on borosilicate glass was focused on characterization of the local environment of radioactive actinides that had been loaded into the glass matrix. Radiation-induced changes in local structure were probed by laser excitation and X-ray spectroscopy. The glass matrix was prepared with B_2O_3 (12%), SiO_2 (63.2%), Na_2O (20%), Al_2O_3 (4.8%). The absence of peaks in the Cu Kα X-ray diffraction pattern from this material confirmed the absence of crystalline phases. Samples that contained the actinide elements of U, Pu, Am, Cm, Bk, and Cf were prepared and studied in laser and X-ray experiments. The results from the samples that contained U and Cm have been analyzed in detail.

a. Local structure of actinides in borosilicate glass

To investigate radiation effects on structural stability, molecular scale structure must be determined before damage occurs. Using laser and X-ray spectroscopic techniques and computational modeling, we have investigated the local structure and chemical bonding of actinide ions at low concentration in borosilicate glass. Our work has shown that these actinide ions have a locally ordered environment in the borosilicate glass samples that we prepared, although, as expected, there is no long-range ordering.

It is well known that optical transitions between 5f states of an actinide ion are most strongly influenced by the nearest neighbor ligands of the actinide ion [Zhorin and Liu 1998]. Such transitions therefore carry information about the immediate structure that surrounds actinide ions in a glass matrix. Selective laser excitation and fluorescence spectra of actinide ions were recorded and analyzed using crystal field theory. These spectra show clear crystal field splitting which is the hallmark of a crystalline local environment for actinide ions. With an exchange charge model of crystal field theory [Liu et al. 1998c, 2000b], we have established a connection between the electronic energy level structure and crystalline structure of Cm^{3+} in this glass matrix. Uranium in borosilicate glass may have different oxidation states depending on firing conditions [Eller and Jarvinen 1985]. For uranium-doped glass samples that were fired in air, the dominant uranium oxidation state is 6+ and such uranium ions are present as uranyl UO_2^{2+} that is directly coordinated with four other oxygen ions in the glass. Evidence of U^{4+} was observed in optical absorption spectra, but there was no evidence of a U^{4+} contribution to the X-ray absorption spectrum, which suggests that the number of U^{4+} is less than 5% of the total uranium ions in our samples. Based on the observed emission spectra, the emitting charge transfer state of UO_2^{2+} strongly couples to the stretching vibrational modes of uranyl. The local environment surrounding UO_2^{2+} also has a modest influence on its electronic and vibrational energies. Our analyses of the observed UO_2^{2+} optical spectra have provided evidence as to its immediate environments in borosilicate glass.

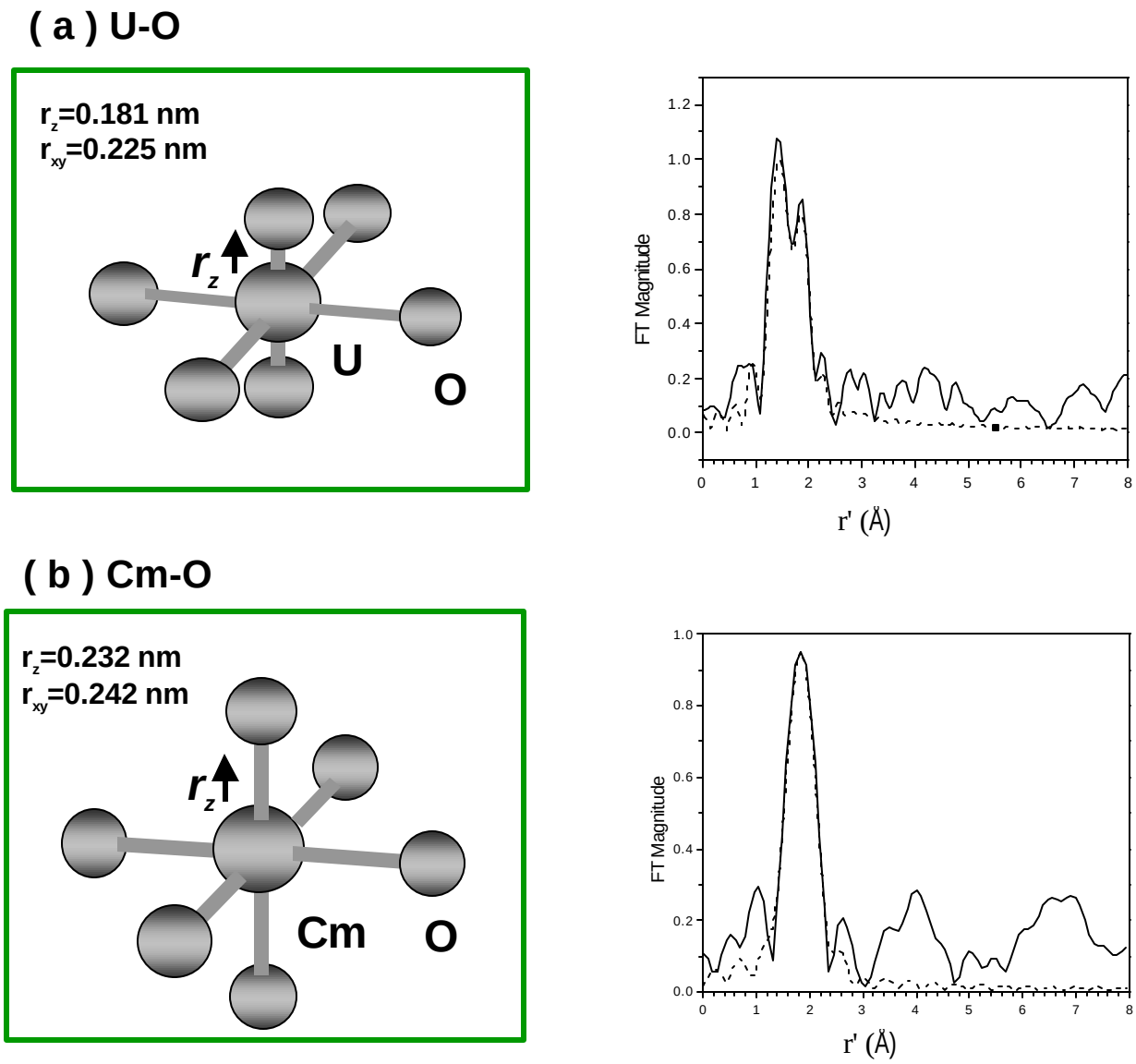

Fig. 8 Nearest-neighbor-ligand structure for (a) U^{6+} and (b) Cm^{3+} in borosilicate glass determined from EXAFS (right panels) and laser spectroscopy [Liu et al. 2000a]. r_z and r_{xy} are the bond lengths between U (Cm) and O in the axial and equatorial directions, respectively.

In studies that complemented our laser investigations, we conducted X-ray spectroscopic measurements and analyzed the observed EXAFS spectra for Cm^{3+} and U^{6+}. Analysis of the X-ray spectra confirmed the observation from laser experiments that these actinide ions have well-defined nearest coordinated ligands and determined the bond lengths for Cm^{3+} and U^{6+} ions and their six directly coordinated oxygen neighbors. Based on analyses of laser and X-ray spectra and related theoretical modeling, we have established a local structure model for Cm^{3+} ions in which six directly coordinated oxygen ions form a tetragonal structure surrounding the actinide ion, with the two axial oxygen ions at a longer distance. [Liu et al.

2000a] The structure of the four equatorial nearest neighbor oxygen surrounding uranyl varies slightly from site to site.

b. Radiation damage in borosilicate glass

As we discussed above, monitoring radiation-induced local structure change is possible for actinides in borosilicate glass where the nearest neighbor ligands of the actinide ions have ordered structure. Optical spectra obtained from laser excitation and X-ray absorption provide "fingerprints" of local structure and structure change. The glass sample doped with 1% ^{244}Cm are expected to accumulate structural damage faster than other samples we prepared. Fig. 8 (a) shows line broadening of the Cm^{3+} self-luminescence that was emitted from the Cm^{3+} ions after electronic excitation induced by α-decay of vicinal Cm^{3+} ions. The narrower line was recorded immediately after the sample was prepared and the broader line was recorded 18 months later. Cascade displacements led a line-width increase

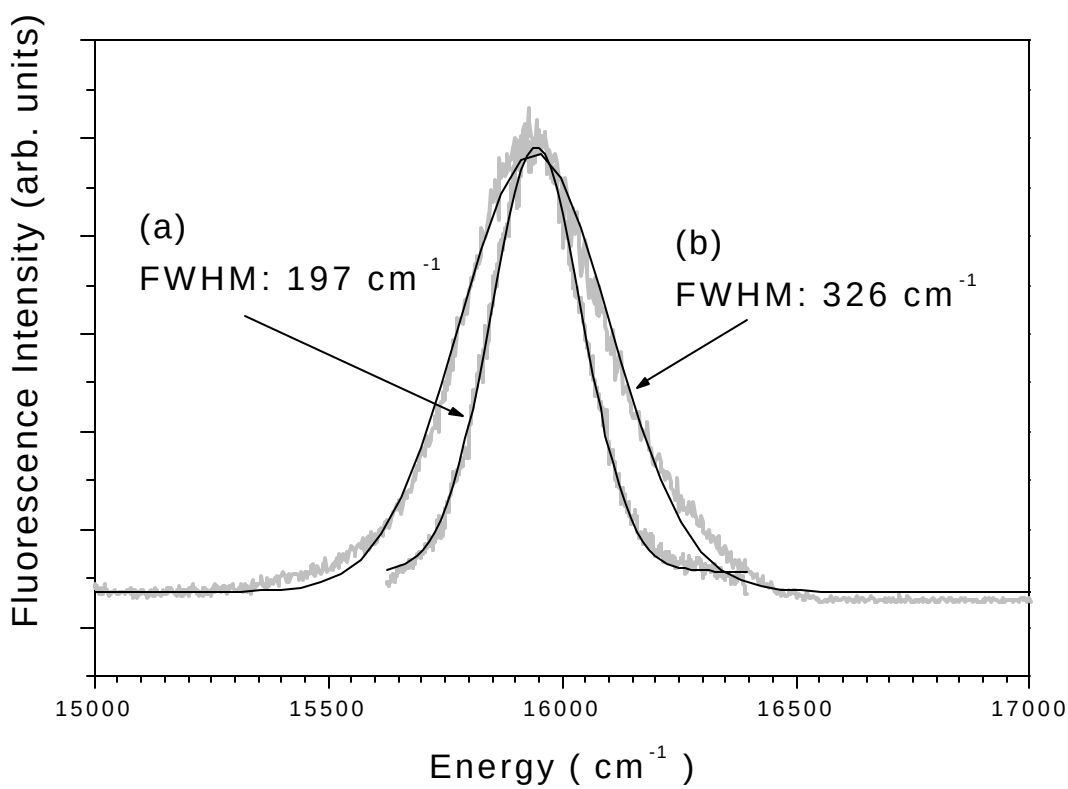

Fig. 9 Radiation-damage-induced inhomogeneous line broadening in ^{244}Cm-doped borosilicate glass. The self fluorescence rises from the electronic transition between the $^{6}D_{7/2}$ and $^{8}S_{7/2}$ states of Cm^{3+}, and is excited by α-decay-induced ionization. The line width was measured as the full width at half maximum intensity (FWHM) at 4 K for (a) when the sample was prepared, and (b) after 18 months of the synthesis. The thin black curves are Gaussian fitting to the experimental data.

from 197 cm^{-1} to 326 cm^{-1}, which indicates a significant increase in structure disorder. Radiation-induced structure disorder is evident also in excitation spectra from the same sample. EXAFS spectra are to be recorded for samples that contain accumulated damage. With experimental data obtained for different radiation doses and using the same method as we used for determining the initially undamaged local structure, we are attempting to model α-decay induced structural changes in borosilicate glass. In our future work, MD simulation will be applied to simulate the behavior of a glass matrix with embedded α-emitting constituents.

V. Implications

In the ^{244}Cm-doped orthophosphate crystals that we studied, microscopic radiation effects were manifested by (i) the presence of dense arrays of individual defect clusters, which are attributed to highly disordered fission tracks, and (ii) the formation of helium bubbles of 5 to 20 nm diameter that most likely result from accumulation of helium generated during α-decay events. These bubbles were rather mobile and easily coalesced under the electron beam exposure. Despite the high accumulated dose, these samples remained largely crystalline. Because lanthanide orthophosphates are known to be highly susceptible to amorphization, this finding suggests that a recovery process must have occurred simultaneously as damage was produced, approximately at a rate comparable to that of damage production. The high recoverability of this material is ascribed to ionization annealing, as well as thermally activated and diffusion-driven annealing processes.

Most models of susceptibility to amorphization ignore kinetics and can only be applied at temperatures so low that point defects are presumably immobile. At higher temperatures, the production of damage during irradiation will be mitigated by simultaneous recovery processes, such as point-defect migration and annealing, or epitaxial re-crystallization at the crystalline-amorphous boundaries [Weber et al. 1989]. The actual amorphization in a crystal will then be influenced by the kinetics of the damage production as well as recovery processes. The fact that the crystallinity in the Cm-doped $LuPO_4$ and YPO_4 was nearly intact after 18 years clearly indicates that the rate of amorphization in this material is probably equal to, or even slightly less than, the rate of recovery, and that damage resulting from α-decay events is probably repaired simultaneously. Previous studies showed that complex effects are associated with ionization, which may contribute to damage accumulation or enhance defect recombination and recovery depending on the materials and the nature of ions employed. [Meldrum et al. 1997, Sales et al. 1992] A recent study [Ouchani et al. 1997] reported recovery of extended defects in a pre-damaged fluorapatite upon helium-ion irradiation, providing direct evidence for ionization annealing. The recovery of extended defects by irradiation with high-energy helium ion is attributed to increased defect mobility induced by electronic energy loss, during which the existing damage along the trajectory of an α particle is believed to be annealed through electronic interactions.

The lack of amorphization that we have observed in our studies of self-radiation damaged crystals is contrary to the results from ion-implantation experiments that indicated that

amorphization should occur below a critical temperature as the radiation dose increases to a critical dose level. Meldrum et al. [1997] have determined, using 800 keV Kr^+ ions, that the critical temperature of amorphization for $LuPO_4$ is about 577 K. However, our results indicate that $LuPO_4$ at room temperature has high recoverability from á-induced radiation damage and suggest that the self-radiation damage over the long-term may not be accurately characterized with parameters such as critical temperature, that were determined based on heavy ion implantation experiments. Apparently, the long-term effects of á-decay events are very different from those in the krypton-ion-implantation experiments. The doped á-emitting actinide ions in the samples generate a relatively low rate of radiation dose that persists for the lifetime of the isotope, whereas in an ion-implantation experiment, an intense flux of high-energy ions, such as Kr^+ or Xe^+, bombards a small area on the sample for a short period of time. Differences are anticipated because there exist collective lattice dynamics for annealing radiation-induced structural defects.

Because of resistance to amorphization under self-radiation, ceramic phosphates are very attractive materials for hosting long-lived α-emitting radionuclides, such as Pu isotopes. However, further investigation is required to evaluate the effects of defect aggregation and mobilization, which will certainly increase the leach rate of such radionuclides and influence the long-term stability of the waste forms.

VI. Publications

Liu, G. K., J. S. Lou, S. T. Li, C. -K. Loong, M. M. Abraham, J. V. Beitz, J. K. Bates, L. A. Boatner, "Self-Radiation Induced Anisotropic Structure Damage in ^{244}Cm-Doped Othophosphate $LuPO_4$ " in *Scientific Basis for Nuclear Waste Management XXI*, **Mat. Res. Soc. Symp. Proc. 506**, 921-922(1998).

Liu, G. K., S. T. Li, J. V. Beitz, M. Abraham, "Effects of Self-Radiation Damage on Electronic Properties of $^{244}Cm^{3+}$ in an orthophosphate Crystal of YPO_4", **J. Alloys & Compounds, 271/273,** 872-875 (1998).

Liu, G. K., S. T. Li, V. V. Zhorin C. -K. Loong, M. M. Abraham, L. A. Boatner, " Crystal-Field Splitting, Magnetic Interaction, and Vibronic Excitations of ^{244}Cm in YPO_4 and $LuPO_4$", **J. Phys. Chem**, **109**, 6800-6808(1998).

Liu, G. K., V. V. Zhorin, M. R. Antonio, S. T. Li, C. W. Williams, and L. Soderholm, "Studies of Local Structure of Cm^{3+} in Borosilicate Glass Using Laser and X-Ray Spectroscopic Methods and Computational Modeling", **J. Chem. Phys**. **112**, 1489-1496 (2000).

Liu, G. K., V. V. Zhorin, S. T. Li, and J. V. Beitz, " Crystal Field Analysis and Monte Carlo Simulation of Lattice Disordering for Cm^{3+} in YPO_4 and $LuPO_4$", **J. Chem. Phys**.112, 373-382(2000).

Luo, J. S. and G. K. Liu, " Microscopic Effects of Self-Radiation Damage in ^{244}Cm-Doped Lanthanide Orthophosphate Crystals", **J. Mater. Res.** (submitted, 1999).

Zhorin,V. V. and G. K. Liu, " Modeling Crystal-Field Interaction for f-Elements in $LaCl_3$", **J. Alloys & Compounds 275/277,** 137-141(1998).

VII. Reference

Abraham, M. M., and L. A. Boatner, Phys. Rev. B **26,** 1434(1982).

Allen, M.P., D.J.Tildesley, *Computer Simulation of Liquids*, Oxford University Press, Oxford, 1987.

Beeler Jr., J.R., *Radiation Effects Computer Experiments*, North-Holland, Amsterdam, (1983).

Boatner, L. A., M. M. Abraham, and M. Rappaz, Sci. Bas. Nuc. Was. Man. 3, 181(1981).

Bourgoin, J. C. and J. W. Corbett, Radiat. Eff. **36**, 157(1978).

Crocombette, J.P., D.Ghaleb, Scientific Basis for Nuclear Waste Management XXI, edited by I.G.McKinley and C.McCombie (Mater. Res. Soc. Symp. Proc**. 506**, Warrendale, PA, 1998) p. 101-108.

Catlow, C.R.A., Ann. Rev. Mater. Sci. **16**, 517 (1986).

Caturla, M.J., N.Soneda, E.Alonso, B.D.Wirth, T.Diaz de la Rubia, J.M.Perlado, J. Nucl. Mater. **276**, 13-21, (2000).

Chung, H. M., W. E. Ruther, J. E. Sanecki, A. Hins, N. J. Zaluzec, and T. F. Kassner, J. Nucl. Mater. **239**, 61(1996).

Delaye, J.M., D.Ghaleb, J. Non-Cryst. Solids **195**, 239-248, (1996).

Eller, P. G., G. D. Jarvinen, J. D. Purson, R. A. Penneman, R. R. Ryan, F. W. Lytle, and R. B. Greegor, Radiochimica Acta **39**, 17(1985).

Ewing, R.C., and T.J. Headley, J. Nuclear Materials **119**, 102(1983).

Ewing, R.C., W.J. Weber, and F.W. Clinard, Jr., Progress in Nuclear Energy **29**, 63(1995).

Evans, D.J., G.P.Morriss, Computer Physics Reports 1, 297-343(1984).

Feuston, B.P., S.H.Garofalini, J. Chem. Phys. 89, 5818 (1988).

Gong, W.L., L.M. Wang, R.C. Ewing, L.F.Chen, and W. Lutze, Mat. Res. Soc. Symp. Proc. **465**, 649(1997).

Griscom, L., L. W. Hobbs, A. Navrotsky, D. L. Price, A. M. Stoneham, and M. C. Harding, J.H., Rep. Prog. Phys. **53**, 1403 (1990)

Heinisch, H.L., B.N.Singh, T.Diaz de la Rubia, J. Nucl. Mater. **212-215**, 127-131, (1994).

Heinisch, H.L., B.N.Singh, J. Nucl. Mater**. 232**, 206-213(1996).

Hobbs, L. W. F. W. Clinard, S. J. Zinkle, and R. C. Ewing, J. Nuc. Mat. **216**, 291(1994).

Inagaki, Y., H. Furuya, K. Idemitsu, T. Banba, S. Matsumoto, and S. Muraoka, Mat. Res. Soc. Symp. Proc. **257**, 199 (1992).

Kot. K, W., N. M. Edelstein, M. M. Abraham, and L. A. Boatner, Phys. Rev. B**48,** 12704(1993).

Leeuw, S. W. de, J. W. Perram, and E. R. Smith, Proc. R. Soc. London, A**373**, 27(1980).

Liu, G. K., J. S. Lou, S. T. Li, C. -K. Loong, M. M. Abraham, J. V. Beitz, J. K. Bates, L. A. Boatner, Scientific Basis for Nuclear Waste Management XXI, Mat. Res. Soc. Symp. Proc. **506**, 921-922(1998a).

Liu, G. K., S. T. Li, J. V. Beitz, M. Abraham, J. Alloys & Compounds **271/273,** 872-875 (1998b).

Liu, G. K., S. T. Li, V. V. Zhorin C. -K. Loong, M. M. Abraham, L. A. Boatner, " J. Phys. Chem. **109**, 6800-6808(1998c).

Liu, G. K., V. V. Zhorin, M. R. Antonio, S. T. Li, C. W. Williams, and L. Soderholm, J. Chem. Phys. **112**, 1489-1496 (2000a).

Liu, G. K., V. V. Zhorin, S. T. Li, and J. V. Beitz, J. Chem. Phys.112, 373-382(2000b).
Lumpkin,G. R. and R. C. Ewing, Phys. Chem. Minerals **16**, 1 (1988).
Luo, J.S., and D.P. Abraham, Proceedings of microscopy and microanalysis **1999**, ed., G.W. Bailey et al., Springer , New York, 848(1999).
Luo, J. S. and G. K. Liu, J. Mater. Res. (submitted, 1999).
Malow, G. and H. Anderson, Scientific basis for nuclear waste management, Vol. 1, ed., G.J. MaCarthy, Plenum Press, New York, 109(1979).
Meldrum, A., L.A. Boatner, and R.C. Ewing, J. Mater. Res. **12**, 1816(1997).
Meldrum, A., L.A. Boatner, and R.C. Ewing, Phys. Rev. B**56**, 13805(1997b)
Meldrum, A., L.A. Boatner, W. J. Weber, and R.C. Ewing, Geoch. Et Cosm. Acta **62**, 2509(1998).
Ouchani, S., J.-C. Dran, J. Chaumont, Nucl. Inst. Meth. Phys. Res. **132B**, 447(1997).
Rapaport, D.C., *The art of molecular dynamics simulation*, Cambridge University Press, Cambridge, 1995
Reid, N. and J.E. Beesley, *Sectioning and cryosectioning for electron microscopy*, Elsevier, New York (1991).
Robinson, M.T., J. Nucl. Mater. **216**, 1-28, (1994).
Sales, B.C., R.A. Zuhr, J.C. McCallum, and L.A. Boatner, Phys. Rev. B**46**, 3215(1992).
Soneda, N., T.Diaz de la Rubia, Philos. Mag. A**78**, 995-1019(1998).
Soules, T.F., A.K.Varshneya, J. Am. Ceram. Soc. **64**, 145 (1981).
Stillinger, F.H., T.A.Weber, Phys. Rev. B**31**, 5262-5271(1985).
Wang, L. M., and L. R. Ewing, Nul. Inst. Meth. Phys. Re. B**65**, 324-329(1992).
Weber, W.J., J. W. Wald, and Hj. Matzke, J. Nuclear Materials **138**, 196(1986).
Weber, W.J., J. Mater. Res**. 5**, 2687(1990).
Weber, W. J., R. C. Ewing, C. A. Angell, G. W. Arnold, A. N. Cormack, J. M. Delaye, D. Weber,W. J., J. Mater. Res**. 5**, 2687(1990).
Weber, W. J. and R. C. Ewing, Mat. Res. Soc. Symp. Proc. **353**, 1389(1995).
Weber, W. J., R. C. Ewing, C. A. Angell, G. W. Arnold, A. N. Cormack, J. M. Delaye, D. L. Griscom, L. W. Hobbs, A. Navrotsky, D. L. Price, A. M. Stoneham, and M. C. Weinberg, J. Mater. Res. **12**, 1946(1997).
Weber, W.J., R.C. Ewing, C.R.A.Catlow, T.Diaz de la Rubia, L.W.Hobbs, C.Kinoshita, Hj.Matzke, A.T.Motta, M.Nastasi, E.K.H.Salje, E.R.Vance, S.J.Zinkle, J. Mater. Res., **13**, 1434-1484(1998).
Weinberg, J. Mater. Res. **12**, 1946(1997).
Woodcock, L. V. and K. Singer, Trans. Faraday Soc. **67**, 12(1971).
Zhuang, H.-Z., X.-W.Zou, Z.-Z.Jin, D.-C.Tian, Phys. Rev. B**52**, 829-832, (1995).
Zhorin,V. V. and G. K. Liu, J. Alloys & Compounds **275/277,** 137-141(1998).
Zinkle, S.J., Nucl. Inst. Meth. Phys. Res. B**91**, 234(1994).